

ActivePose: Active 6D Object Pose Estimation and Tracking for Robotic Manipulation

Sheng Liu^{1,5}, Zhe Li², Weiheng Wang¹, Han Sun^{*2},
Heng Zhang³, Hongpeng Chen⁴, Yusen Qin⁵, Arash Ajoudani³, Yizhao Wang^{†2}

Abstract—Accurate 6-DoF object pose estimation and tracking are critical for reliable robotic manipulation. However, zero-shot methods can fail under viewpoint-induced ambiguities, and fixed-camera setups struggle when objects move or become occluded. We propose *ActivePose*, a closed-loop system that (i) actively disambiguates zero-shot pose estimates and (ii) actively tracks poses during downstream manipulation.

For active pose estimation, we combine a vision-language model (VLM) with CAD-based “robot imagination.” Offline, we render CAD views, compute FoundationPose hypothesis entropy from rendered views, and build a geometry-aware prompt with low-entropy (unambiguous) and high-entropy (ambiguous) exemplars. Online, the system queries the VLM for the ambiguity probability of the current view; when ambiguous, it renders virtual views from an IK-feasible candidate set, scores each view by fusing VLM-predicted ambiguity and entropy-based uncertainty, and executes the selected Next-Best-View (NBV) for disambiguation.

For active pose tracking, we train a diffusion policy via imitation learning to generate receding-horizon camera trajectories that preserve target visibility and reduce pose-loss under object motion and occlusions. Experiments in simulation and on real robots demonstrate consistent improvements over classical baselines.

I. INTRODUCTION

6D object pose estimation, which recovers an object’s translation and rotation relative to the camera, plays a pivotal role in robotic manipulation tasks such as grasping [1], [2], [3] and assembly [4]. Previous works [5], [6], [7], [8], [9], [10] achieved strong performance by training on specific datasets. More recently, zero-shot methods [11], [12], [13] demonstrated the ability to estimate poses for novel objects using only their CAD models, without requiring additional real-world annotations.

Despite their strong performance, most existing methods assume that the observation from a single viewpoint contains enough cues to estimate a unique pose. In practice, however, self-occlusion and inter-object occlusion frequently obscure distinctive regions, resulting in fundamentally ill-posed estimation problems. This challenge is especially prevalent in industrial metal parts, where symmetric structures and textureless surfaces inherently reduce distinctive regions, leading to severely exacerbated pose ambiguity.

Since pose ambiguity is inevitable in practical scenarios, resolving it becomes critically important. While physically

reorienting the target object or removing occluders can resolve pose ambiguity, such direct interventions are often prohibited in tasks involving high-precision components or delicate instruments. Instead, enabling cameras to actively adjust viewpoints, which mimics human observation, offers a more versatile solution.

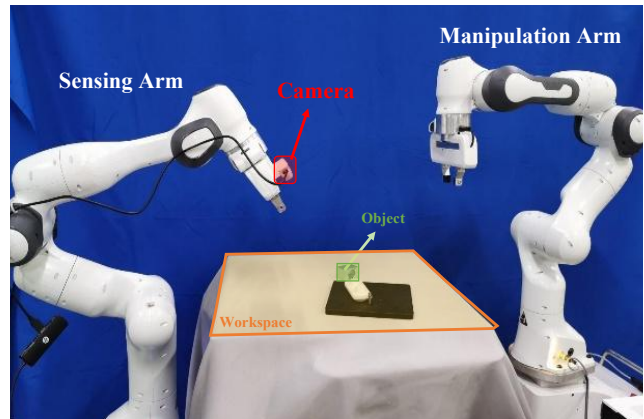


Fig. 1: Dual-arm experimental setup. The left arm serves as the *sensing arm* and carries a wrist-mounted RGB-D camera, while the right arm serves as the *manipulation arm* equipped with a parallel-jaw gripper.

Although prior studies [14], [15] attempted to predict pose ambiguity, they not only depend on costly prior information, but they also fail to provide actionable solutions for ambiguity elimination. Several methods have trained neural networks to predict the Next-Best-View (NBV) for active pose estimation [16], [17], [18]. Although these approaches show promise, they require extensive offline training. Thus, determining optimal camera movements to mitigate pose ambiguity during operation remains an open and challenging problem.

With this motivation, we propose *ActivePose*, a closed-loop framework for zero-shot 6D pose disambiguation and downstream pose tracking. We ground a VLM with entropy-ranked CAD renderings to detect viewpoint-induced ambiguity and select NBVs from a small IK-feasible candidate set via renderer-based view synthesis. We further learn a diffusion-policy tracker to actively maintain visibility under motion and occlusions.

To our knowledge, *ActivePose* is among the first closed-loop frameworks that combines zero-shot ambiguity detection with feasible NBV selection for CAD-based novel-

* Han Sun is the project leader.

† Yizhao Wang is the corresponding author.

Authors Affiliation: ¹Karlsruhe Institute of Technology, Germany, ²Shanghai Jiao Tong University, China, ³Istituto Italiano di Tecnologia, Italy, ⁴The Hong Kong Polytechnic University, Hong Kong, ⁵D-Robotics, China.

object pose estimation, and further integrates active tracking for downstream manipulation under motion and occlusions. For the benefit of the research community, we will release our code as open source.

In summary, our contributions are:

- A zero-shot active pose estimation module that detects viewpoint ambiguity and executes feasible NBV moves to disambiguate CAD-based 6D pose estimates in closed loop.
- A demonstration-trained diffusion-policy tracker that generates camera trajectories to prevent pose-loss under motion and occlusions.
- Evaluation in simulation and on real dual-arm hardware, including an industrial peg-in-hole assembly case study and a runtime analysis of VLM latency.

II. RELATED WORK

A. 6D Pose Estimation

In recent years, 6D pose estimation methods based on a single RGB-D image using neural networks [5], [6], [7], [19], [20], [21] have outperformed the classic approaches [22]. However, these methods did not consider the ambiguous pose from a specific viewpoint. To address this, active pose estimation techniques adjust the camera viewpoint to improve overall confidence—but they typically rely on object-specific training, hand-crafted heuristics, or expensive annotations [16], [17], [18]. Differently, we target *zero-shot* ambiguity detection and disambiguation for novel CAD objects: we ground a VLM with entropy-ranked CAD renders to assess geometric ambiguity, and select NBVs from a feasible candidate set via renderer-based view synthesis (“robot imagination”) in a closed loop.

B. Vision-Language Models for Robotics

The rapid development of VLMs has further advanced the field of robotics, enabling intelligent agents to interpret natural language commands and reason about visual scenes in a generalizable, task-independent manner [23]. A key advantage of these basic models is that they have been pre-trained on large-scale datasets and can usually be directly deployed in robot systems as high-level planners [24], [25], [26] or low-level controllers [27], [28], [29] without having to learn from scratch, which significantly reduces training costs and improves generalization capabilities. In our work, we use a VLM not as a task planner, but as a *geometric ambiguity assessor*: grounded by geometry-aware exemplars, it outputs an ambiguity probability for the current view and helps rank candidate viewpoints for zero-shot active disambiguation.

C. Diffusion Models for Robotics

Diffusion models have recently emerged as a powerful paradigm for robot learning, particularly for manipulation, by modeling complex and multimodal action or trajectory distributions and generating smooth behaviors through iterative denoising [30]. A representative approach, Diffusion Policy [31], formulates visuomotor control as a conditional diffusion

process that predicts action sequences and executes them in a receding-horizon loop, achieving strong performance across diverse manipulation benchmarks.

In contrast to prior diffusion-based manipulation policies that primarily generate end-effector motions for task execution, we use a diffusion policy as an *active sensing* component: the policy generates receding-horizon camera trajectories that maintain target visibility and reduce pose-loss under object motion and occlusions during downstream manipulation.

III. PROBLEM FORMULATION

We formulate active 6D object pose estimation and tracking as a two-stage closed-loop problem. Given a CAD model, an initial camera pose, and a live RGB-D stream, the system first performs *active pose estimation*: it detects viewpoint-induced ambiguity using a VLM grounded by geometry-aware exemplars together with FoundationPose hypothesis entropy, and, when ambiguous, moves the camera to a next-best view selected by ranking rendered candidates to obtain an unambiguous pose. After obtaining this disambiguated pose, the system performs *active pose tracking* during manipulation: a diffusion-policy tracker generates camera trajectories to preserve visibility and prevent pose-loss under object motion and occlusions.

IV. METHOD

Our approach comprises two tightly integrated modules: an active pose estimation pipeline that resolves viewpoint-induced 6D pose ambiguities (Algorithm 1), and an active pose tracking module that actively moves the camera to preserve visibility and prevent pose-loss under motion and occlusions (Algorithm 2).

A. Active Pose Estimation

Our active pose estimation pipeline (see Fig. 2) comprises two stages: (i) *offline* geometry-aware prompt construction and (ii) *online* ambiguity detection with feasible NBV selection.

Offline: We pre-render K canonical views $\{R_k\}_{k=1}^K$ by sampling camera poses on a tabletop-facing hemisphere around the object (fixed standoff distance d , camera optical axis pointing to the object center), and reuse these renders to construct a geometry-aware prompt that remains fixed for all online queries of the same object. These canonical views are used only for prompt construction and do not need to be kinematically feasible for the robot. For each rendered view R_k , we invoke FoundationPose [12] to obtain the top- N 6D pose hypotheses $\{\hat{T}_i\}_{i=1}^N$ with associated confidence weights $\{w_i\}_{i=1}^N$. We normalize the weights to form a discrete distribution $p_i = \frac{w_i}{\sum_{j=1}^N w_j}$ and compute the *normalized* Shannon entropy

$$\bar{H}(R_k) = \frac{-\sum_{i=1}^N p_i \log p_i}{\log N} \in [0, 1]. \quad (1)$$

This serves as a geometry-driven uncertainty score that is comparable across views. We then select two small subsets:

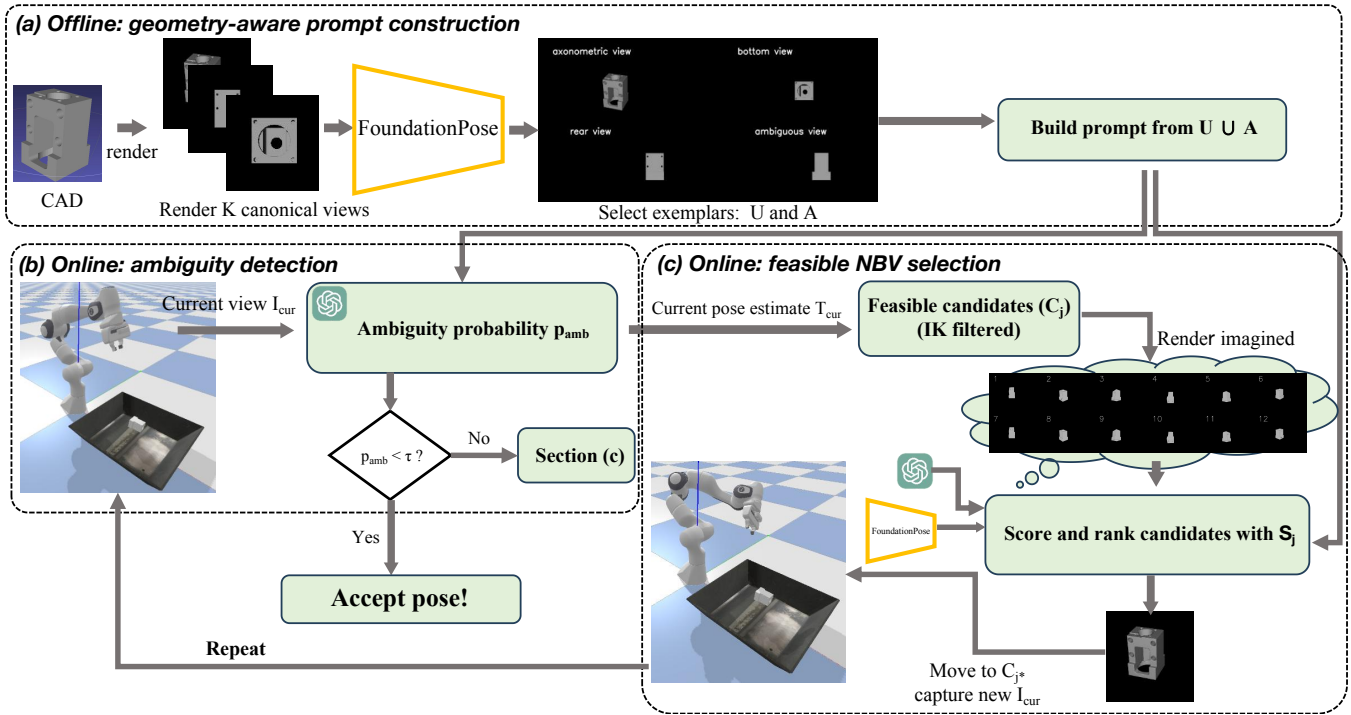


Fig. 2: **Active pose estimation.** (a) Offline: render canonical CAD views, compute the hypothesis entropy of FoundationPose, and build a geometry-aware prompt from low-/high-entropy exemplars. (b) Online: compute VLM ambiguity p_{amb} for the current view and trigger disambiguation when $p_{\text{amb}} > \tau$. (c) Rank feasible candidate views using rendered imagined observations and the fused score, execute the selected NBV, and repeat to budget L .

U as the K_u lowest-entropy *unambiguous* views and A as the K_a highest-entropy *ambiguous* views. The geometry-aware prompt is constructed by aggregating the images in $U \cup A$ with a fixed instruction template.

Online: Given the current observation I_{cur} , we estimate an initial pose $T_{\text{cur}} = \text{FoundationPose}(I_{\text{cur}})$ and compute an ambiguity probability p_{amb} using a fixed, per-object prompt (constructed offline) and constrained $\{\text{Yes}, \text{No}\}$ log-probabilities from the VLM:

$$\begin{aligned}
 p_{\text{amb}} &= P_{\text{VLM}}(\text{Yes} \mid I_{\text{cur}}, \text{prompt}) \\
 &= \frac{\exp(\ell_{\text{Yes}})}{\exp(\ell_{\text{Yes}}) + \exp(\ell_{\text{No}})}.
 \end{aligned} \tag{2}$$

If $p_{\text{amb}} < \tau$, we directly output T_{cur} ; otherwise we iteratively select a feasible NBV within a small budget L . A larger τ makes disambiguation less frequent (only highly ambiguous views trigger NBV), while a smaller τ triggers NBV more aggressively. Given the current camera pose bT_c and the current pose estimate T_{cur} , the generator \mathcal{G} samples M local candidate camera poses around the object and retains only IK-feasible candidates. For each feasible candidate C_j , we render an imagined view \hat{I}_j and compute $p_{\text{amb},j} = P_{\text{VLM}}(\text{Yes} \mid \hat{I}_j, \text{prompt})$ with the same prompt. We score candidates by $S_j = \lambda \bar{H}(\hat{I}_j) + (1 - \lambda) p_{\text{amb},j}$, then move the camera to the best-scoring candidate view, and acquire a new real observation. We repeat this process until the newly acquired image yields $p_{\text{amb}} < \tau$ or the budget L is exhausted (Algorithm 1); at termination, we return the current estimate

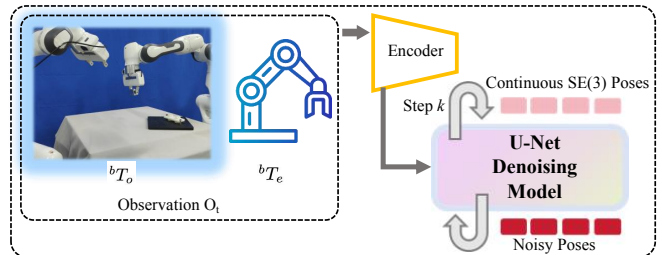


Fig. 3: **Active pose tracking.** The policy encodes the current observation O_t , denoises over K_d reverse-diffusion steps to generate a horizon of continuous SE(3) poses, and executes the last k_h poses in a receding-horizon loop.

as the final pose T_o .

B. Active Pose Tracking

After obtaining the final disambiguated pose T_o from active pose estimation, we formulate active tracking as a *conditional diffusion* problem to maintain continuous visibility (see Fig. 3). Because the camera is rigidly mounted on the sensing end-effector with a fixed extrinsic eT_c , a predicted end-effector trajectory $\{{}^bT_{e,t}\}$ uniquely induces a camera trajectory $\{{}^bT_{c,t}\}$ via ${}^bT_c = {}^bT_e \cdot {}^eT_c$. For clarity, we learn and execute end-effector trajectories, which are equivalent to camera trajectories under this rigid mounting.

At each time step t , the pose estimator provides the object pose in the camera frame cT_o . We convert it to the robot base

Algorithm 1 Active Pose Estimation

Require: CAD model; ambiguity threshold τ ; fusion weight λ ; NBV budget L ; candidate-view generator $\mathcal{G}(\cdot)$ with IK filtering

Ensure: final 6D object pose in camera frame cT_o

- 1: **Offline:**
- 2: Render K canonical views $\{R_k\}_{k=1}^K$
- 3: Compute normalized pose entropies $\{\bar{H}_k\}_{k=1}^K$ from FoundationPose hypotheses (Eq. (1))
- 4: $U \leftarrow K_u$ lowest-entropy views; $A \leftarrow K_a$ highest-entropy views
- 5: prompt \leftarrow BUILDPROMPT(U, A)
- 6: **Online:**
- 7: Acquire I_{cur} at current camera pose bT_c
- 8: $T_{\text{cur}} \leftarrow$ FoundationPose(I_{cur})
- 9: **for** $\ell = 0$ **to** L **do**
- 10: $p_{\text{amb}} \leftarrow$ AMBIGUITYPROB($I_{\text{cur}}, \text{prompt}$) (Eq. (2))
- 11: **if** $p_{\text{amb}} < \tau$ **or** $\ell = L$ **then**
- 12: **break**
- 13: **end if**
- 14: ${}^bT_o \leftarrow {}^bT_c \cdot T_{\text{cur}}$
- 15: $\{C_j\}_{j=1}^M \leftarrow \mathcal{G}({}^bT_c, {}^bT_o)$
- 16: **for** $j = 1, \dots, M$ **do**
- 17: $\hat{I}_j \leftarrow$ Render(C_j)
- 18: $p_{\text{amb},j} \leftarrow$ AMBIGUITYPROB(\hat{I}_j, prompt) (Eq. (2))
- 19: $\bar{H}_j \leftarrow$ POSENTROPY(\hat{I}_j) (Eq. (1))
- 20: $S_j \leftarrow \lambda \bar{H}_j + (1 - \lambda)p_{\text{amb},j}$
- 21: **end for**
- 22: $j^* \leftarrow \arg \min_j S_j$
- 23: Move camera to C_{j^*} and acquire new real image I_{cur}
- 24: ${}^bT_c \leftarrow C_{j^*}$
- 25: $T_{\text{cur}} \leftarrow$ FoundationPose(I_{cur})
- 26: **end for**
- 27: ${}^cT_o \leftarrow T_{\text{cur}}$

frame using the current end-effector pose bT_e and the fixed camera extrinsic eT_c :

$${}^bT_o = {}^bT_c \cdot {}^cT_o = {}^bT_e \cdot {}^eT_c \cdot {}^cT_o. \quad (3)$$

We then build the observation $O_t = \{{}^bT_o^{t-H+1:t}, {}^bT_e^{t-H+1:t}\}$, containing the past H frames of (i) the object pose in the robot base frame bT_o and (ii) the end-effector pose in the base frame bT_e . We condition the policy on a short history of poses rather than a single-frame estimate, which provides motion context and improves tracking robustness.

Specifically, starting from Gaussian noise $A_t^{K_d}$, the denoising network ε_θ performs K_d reverse-diffusion steps to transform $A_t^{K_d}$ into a noise-free action A_t^0 :

$$A_t^{k-1} = \alpha_k \left(A_t^k - \gamma_k \varepsilon_\theta(O_t, A_t^k, k) \right) + \sigma_k \mathcal{N}(0, I), \quad (4)$$

$$\mathcal{L} = \mathbb{E} \left[\left\| \epsilon^k - \varepsilon_\theta(O_t, \hat{\alpha}_k A_t^0 + \hat{\beta}_k \epsilon^k, k) \right\|^2 \right], \quad (5)$$

where $\alpha_k, \gamma_k, \sigma_k$ are parameters of the noise schedule at

Algorithm 2 Active Pose Tracking

Require: Object pose in camera frame cT_o , initial end-effector pose ${}^bT_{e,1}$, camera pose in end-effector frame eT_c , history length H , prediction horizon K , executed tail length k_h , total steps N .

Ensure: executed poses $\{{}^bT_{e,t}\}_{t=1}^N$

- 1: $t \leftarrow H$
- 2: **while** $t \leq N$ **do**
- 3: Compute object pose in base frame: bT_o (Eq. (3))
- 4: Collect history window: O_t
- 5: Sample a future end-effector pose sequence by denoising:
 $\{{}^b\hat{T}_e^{t+1:t+K}\} \leftarrow \text{DP}(O_t)$
 \triangleright DP denotes the diffusion policy, see Eqs. (4)–(5)
- 6: Select the **last** k_h **poses** of the predicted horizon K :
 $\mathcal{T}_t \leftarrow \{{}^b\hat{T}_e^{t+K-k_h+1:t+K}\}$
- 7: Time-parameterize and interpolate from current bT_e to \mathcal{T}_t , then execute the resulting continuous trajectory via servo control.
- 8: Update bT_e to the last executed pose: ${}^bT_e \leftarrow {}^b\hat{T}_e^{t+K}$
- 9: $t \leftarrow t + k_h$
- 10: **end while**

step k , ϵ^k is the injected noise, and $\hat{\alpha}_k, \hat{\beta}_k$ are the one-step forward diffusion coefficients [32]. Mean squared error (MSE) loss is employed as the objective function to supervise noise prediction (Eq. (5)). The rotation is represented as R6D [33], a continuous 6D representation for $SO(3)$ that avoids discontinuities and is empirically stable for generative modeling. At runtime, the diffusion policy outputs an absolute horizon $\{{}^b\hat{T}_e^{t+1:t+K}\}$. Instead of executing a prefix, we execute the *last* k_h poses $\{{}^b\hat{T}_e^{t+K-k_h+1:t+K}\}$, biasing the camera toward the terminal viewpoint that best preserves future visibility. We interpolate from the current bT_e to this segment for smooth, feasible motion and repeat in a receding-horizon loop.

V. EXPERIMENTS

This section describes the experimental setups, implementation details, evaluation protocol, and quantitative results for active pose estimation and active pose tracking, followed by ablations, runtime analysis, and an engineering case study on peg-in-hole assembly.

A. Experimental Setups

Hardware/Software and Objects. For **active pose estimation**, we evaluate in both simulation and the real world. Simulation is implemented in PyBullet [34], which provides controlled rendering for NBV selection. For **active pose tracking**, we exclusively perform real-robot evaluations to capture realistic occlusions, dynamics, and sensing noise. All real-world experiments use two Franka Emika Panda 7-DOF arms: a *sensing arm* carries a wrist-mounted Intel RealSense D435 RGB-D camera (640×480 at 30 Hz), and

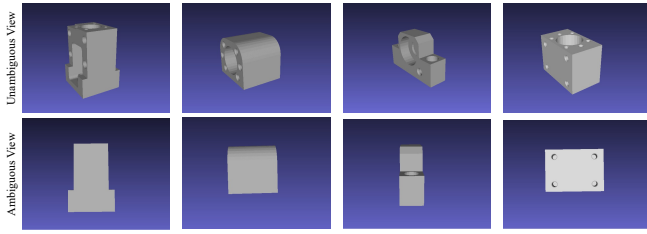


Fig. 4: CAD models of the experimental objects (Obj. 1–3 from MP6D; Obj. 4 for assembly) and an example ambiguous view.

a *manipulation arm* is equipped with a parallel-jaw gripper (see Fig. 1). As shown in Fig. 4, we select three objects from MP6D [35] for evaluation and an additional object for the peg-in-hole assembly task. All four objects exhibit strong viewpoint-induced ambiguities due to symmetry and textureless geometry.

Implementation details. *Active pose estimation:* We call the ChatGPT4o API as our VLM. The VLM operates on a cropped image (resized to 224×224) paired with a fixed, per-object geometry-aware prompt, while FoundationPose uses the full RGB-D observation. VLM inference is run deterministically: we set $\text{temperature} = 0$ (and $\text{top-p} = 1.0$) and compute the ambiguity probability from the returned $\{\text{Yes}, \text{No}\}$ log-probabilities (Eq. (2)); all other decoding options are fixed across experiments. Offline prompting uses $K=48$ rendered views, from which we select $K_u=K_a=2$ exemplars; the ambiguity threshold is fixed to $\tau=0.5$. When ambiguity is triggered, we render $M=12$ feasible candidate viewpoints and score them with fusion weight $\lambda=0.6$. We use fixed $L=3$ across all objects and scenarios.

Prompt template: For each object, the prompt consists of (i) a short instruction asking whether the pose is ambiguous and constraining the answer to $\{\text{Yes}, \text{No}\}$, (ii) K_u low-entropy exemplar renders labeled No and K_a high-entropy exemplar renders labeled Yes , and (iii) the query image.

Active pose tracking: We collect 10 expert demonstrations per task, each consisting of ~ 200 frames of object poses bT_o and end-effector poses bT_e at 10Hz, via teleoperation that keeps the target within the camera frustum. We train the diffusion policy with AdamW (batch size 40, learning rate 3×10^{-4}) for 2,000 epochs. We use fixed $H=5$, $K=10$, $k_h=5$ and $N=200$ across all objects and scenarios. All training and inference run on a single NVIDIA RTX 4090 GPU.

Estimation scenarios. We evaluate active pose estimation under two conditions:

- 1) *Random Placement:* each object is placed at a random position and orientation on the workspace.
- 2) *High-Entropy Placement:* each object is deliberately positioned at a precomputed high-entropy (ambiguous) viewpoint.

Estimation baselines.

- **Fixed-View:** run FoundationPose once at the initial camera pose (no active viewpoint selection).
- **Random-NBV:** upon ambiguity detection, randomly

select one of the M feasible candidate viewpoints for a second FoundationPose estimate.

- **Entropy-NBV:** upon ambiguity detection, select NBV by minimizing the normalized hypothesis entropy \bar{H}_j over the M feasible candidates (no VLM).
- **VLM-NBV:** upon ambiguity detection, select NBV by minimizing VLM ambiguity $p_{\text{amb},j}$ over the M feasible candidates (no FoundationPose).

Estimation metric. We report *success rate* (SR), defined as the percentage of trials whose final estimated 6D pose has translation error below 5 mm and rotation error below 5° . Each method is tested for 100 trials per scenario.

Tracking scenarios. We evaluate all trackers under four challenging conditions:

- 1) *Long-range linear motion:* the object moves along a straight trajectory from point A to point B, where point B is randomized.
- 2) *Circular rotational motion:* the object rotates around a fixed point on the table, inducing large viewpoint changes.
- 3) *Temporary occlusion:* the object is briefly occluded (up to 1 s), requiring recovery upon reappearance.
- 4) *Random spatial motion:* the object undergoes unpredictable translational and rotational motions in 3D, including sharp turns and speed variations.

Tracking baselines.

- **Pose-Servo:** a classical pose-based visual servoing baseline. The wrist-mounted camera provides the current 6D object pose; a proportional controller maps pose error to end-effector velocity commands.
- **World-Camera:** a fixed, calibrated overhead camera continuously tracks the object’s 6D pose via FoundationPose.

Tracking metric. We report *success rate* (SR) per trial: the fraction of runs that complete the scenario without any *pose-loss* event. We declare pose-loss if (i) FoundationPose returns no valid pose for more than 10 consecutive frames, or (ii) the object exits the camera FOV. Each method is evaluated in 50 independent trials per scenario.

B. Experimental Results

Active Pose Estimation Results. We evaluate two placement conditions: *Random Placement* and *High-Entropy Placement* (deliberately ambiguous starts). Unless otherwise stated, SR is averaged over four objects (Obj. 1–4).

Simulation. As reported in Table I, Fixed-View degrades sharply from Random Placement (60.0%) to High-Entropy Placement (20.0%), highlighting strong viewpoint-induced ambiguity. Random-NBV (28.3%) improves over Fixed-View (20.0%), confirming that acquiring an additional view can help, but remains unreliable without guided selection. Entropy-NBV performs competitively under Random Placement (64.3%) but drops under High-Entropy Placement (42.0%), suggesting that hypothesis entropy alone can be an imperfect proxy for selecting a truly disambiguating view. VLM-NBV performs worst among active baselines (41.0% /

TABLE I: Active pose estimation in simulation and on real robots.

Method	Simulation										Real Robots									
	Random Placement					High-Entropy Placement					Random Placement					High-Entropy Placement				
	Obj 1	Obj 2	Obj 3	Obj 4	SR	Obj 1	Obj 2	Obj 3	Obj 4	SR	Obj 1	Obj 2	Obj 3	Obj 4	SR	Obj 1	Obj 2	Obj 3	Obj 4	SR
Fixed-View	70.0%	50.0%	50.0%	70.0%	60.0%	40.0%	10.0%	20.0%	10.0%	20.0%	68.0%	47.0%	42.0%	54.0%	52.8%	26.0%	21.0%	31.0%	9.0%	21.8%
Random-NBV	73.0%	51.0%	66.0%	70.0%	65.0%	41.0%	21.0%	34.0%	17.0%	28.3%	71.0%	52.0%	43.0%	64.0%	57.5%	55.0%	41.0%	67.0%	28.0%	47.8%
Entropy-NBV	65.0%	57.0%	61.0%	74.0%	64.3%	52.0%	38.0%	41.0%	37.0%	42.0%	73.0%	51.0%	50.0%	57.0%	57.8%	60.0%	46.0%	63.0%	26.0%	48.8%
VLM-NBV	67.0%	53.0%	25.0%	19.0%	41.0%	46.0%	34.0%	27.0%	32.0%	34.8%	37.0%	29.0%	23.0%	41.0%	32.5%	31.0%	37.0%	51.0%	10.0%	32.3%
Ours	100.0%	100.0%	100.0%	90.0%	97.5%	100.0%	90.0%	100.0%	90.0%	95.0%	90.0%	90.0%	100.0%	90.0%	92.5%	100.0%	90.0%	100.0%	90.0%	95.0%

TABLE II: Active pose tracking on real robots.

Method	Long-range Linear Motion					Circular Rotational Motion					Temporary Occlusion					Random Spatial Motion				
	Obj 1	Obj 2	Obj 3	Obj 4	SR	Obj 1	Obj 2	Obj 3	Obj 4	SR	Obj 1	Obj 2	Obj 3	Obj 4	SR	Obj 1	Obj 2	Obj 3	Obj 4	SR
Pose-Servo	65.0%	70.0%	60.0%	50.0%	61.3%	0.0%	0.0%	0.0%	0.0%	0.0%	0.0%	0.0%	5.0%	0.0%	1.3%	50.0%	45.0%	50.0%	55.0%	50.0%
World-Camera	50.0%	45.0%	65.0%	35.0%	48.8%	65.0%	60.0%	75.0%	50.0%	62.5%	35.0%	15.0%	15.0%	5.0%	17.5%	70.0%	55.0%	65.0%	45.0%	58.8%
Ours	85.0%	90.0%	80.0%	95.0%	87.5%	80.0%	90.0%	95.0%	100.0%	91.3%	50.0%	45.0%	65.0%	50.0%	52.5%	70.0%	75.0%	65.0%	80.0%	72.5%

TABLE III: Ablation of active pose estimation.

Method	Sim / Random		Sim / High-Entropy		Real / Random		Real / High-Entropy	
	SR	#NBV	SR	#NBV	SR	#NBV	SR	#NBV
Ours (entropy-ranked exemplars, $\lambda=0.6$)	97.5%	0.60	95.0%	0.90	92.5%	0.60	95.0%	1.00
Prompt grounding (exemplars)								
Text-only prompt (no exemplars)	73.0%	1.60	61.0%	1.30	70.5%	1.65	53.0%	2.00
Random exemplars (same count as K_u+K_a)	77.5%	1.10	68.0%	1.00	78.5%	0.90	70.5%	1.10
Fusion sensitivity (sweep λ)								
$\lambda=0$ (VLM-only)	41.0%	2.90	34.8%	3.00	32.5%	2.80	32.3%	3.00
$\lambda=0.3$	47.4%	2.70	36.8%	2.60	31.6%	2.60	25.4%	2.50
$\lambda=0.9$	61.7%	1.30	46.0%	1.40	65.5%	1.40	50.0%	1.70
$\lambda=1$ (entropy-only)	64.3%	1.40	42.0%	1.60	57.8%	1.50	48.8%	1.30

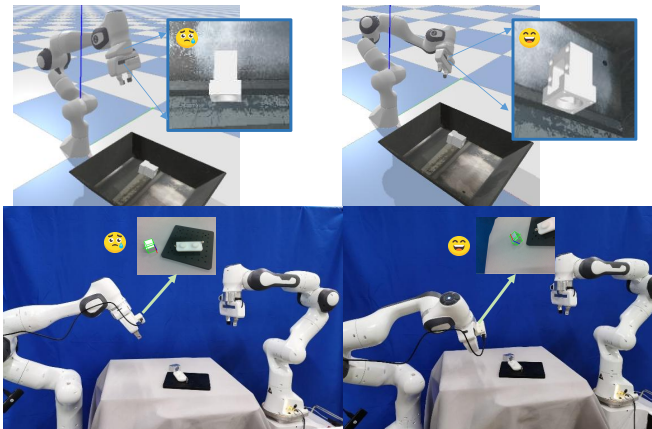


Fig. 5: Example of active pose estimation. An ambiguous initial view triggers NBV selection; moving to the selected viewpoint yields an unambiguous 6D pose estimate, shown in simulation (top) and real-robot trials (bottom).

34.8%), indicating that VLM ambiguity alone is insufficient for reliable NBV ranking over rendered candidates. In contrast, ActivePose (97.5% / 95.0%) achieves consistently high SR in both conditions, demonstrating robust disambiguation (Table I).

Real world. Table I shows a similar trend: Fixed-View (21.8%) and Random-NBV (47.8%) drop substantially under High-Entropy Placement. Entropy-NBV yields moderate gains over Random-NBV in the High-Entropy setting (48.8% vs. 47.8%), while VLM-NBV remains unreliable in the

real world (32.5% / 32.3%), consistent with the simulation results. In contrast, ActivePose achieves the best performance in both placements (92.5% on Random and 95.0% on High-Entropy), indicating robust disambiguation. The lower SR in real-world trials compared to simulation is likely due to real sensing imperfections, including sensor noise and the synthetic-to-real gap between rendered and captured observations. Figure 5 shows an example of active pose estimation, where an ambiguous view triggers NBV selection and a second view resolves the ambiguity.

Active Pose Tracking Results. Table II reports SR in 50 trials per scenario. Across all four motion scenarios, our tracker consistently outperforms Pose-Servo and World-Camera by large margins. Pose-Servo frequently fails due to reachability limitations under large viewpoint changes, while World-Camera fails when the object exits its fixed FOV. Unlike pose-based servoing, which enforces strict instantaneous pose-error tracking and can drive the arm into infeasible motions, our learned policy generates smooth, anticipatory camera motions that prioritize maintaining visibility and reacquiring the target after occlusion. Figure 6 illustrates an example of active pose tracking in our dual-arm setup.

C. Ablation Studies

To isolate the specific value of using a VLM, to examine whether the VLM ambiguity score complements the FoundationPose entropy signal, and to assess the choice of the fusion weight λ , we conduct ablations on the active pose estimation module.



Fig. 6: **Example of active pose tracking.** While the manipulation arm manipulates the object, the sensing arm with a wrist-mounted RGB-D camera actively follows to keep the target in view.

TABLE IV: **Runtime breakdown of active pose estimation.**

Component	Time (ms)
FoundationPose (single view, per image)	60
Render $M=12$ imagined views (total)	80
VLM query (per call, mean \pm std)	600 ± 200
NBV evaluation (12 VLM calls + scoring)	7,500
End-to-end NBV cycle (worst case, incl. motion)	11,000

TABLE V: **Peg-in-hole assembly.**

Method	SR
Fixed-View + World-Camera	40%
Fixed-View + Pose-Servo	50%
Random-NBV + Pose-Servo	70%
Ours	90%

We ablate active pose estimation on the same four objects under both placement conditions, using the same SR metric ($5 \text{ mm} / 5^\circ$) and default settings ($K=48$, $K_u=K_a=2$, $M=12$, $\tau=0.5$, $L=3$). In addition to SR, we report #NBV: the average number of executed NBV actions (additional viewpoints beyond the initial view) per trial. A lower #NBV is better.

Prompt grounding. Table III shows that entropy-ranked exemplars substantially outperform a text-only prompt and random exemplars, improving both SR and #NBV. Random exemplars keep the same exemplar count and labels as the full method, but randomly sample the low-/high-entropy exemplars from their respective pools instead of taking the entropy extremes. Notably, text-only prompting frequently exhausts the NBV budget ($\#NBV \approx 1.3\text{--}2.0$) while still yielding low SR, indicating that exemplars are critical for calibrating the VLM to *geometric* ambiguity.

Fusion sensitivity. Sweeping λ confirms that intermediate fusion ($\lambda=0.6$) provides the best SR-#NBV trade-off. At $\lambda=0$ (VLM-only), the policy often hits the budget limit ($\#NBV \approx 2.5\text{--}3.0$) yet remains inaccurate, showing that VLM ambiguity alone is insufficient for reliable NBV ranking. At $\lambda=1$ (entropy-only), #NBV decreases but SR remains substantially below the fused setting, suggesting that hypothesis entropy alone can be misled by rendering-to-real discrepancies and partial occlusions. Overall, the results support that VLM ambiguity and hypothesis entropy provide complementary cues for selecting disambiguating viewpoints.

D. Runtime Analysis

Querying an external VLM API introduces response delays, which can be a practical limitation for real-time robotics applications. Table IV reports a runtime breakdown of active pose estimation on a workstation with an NVIDIA RTX 4090 GPU. In the worst case (ambiguity detected and all $M=12$ candidates evaluated), one NBV cycle takes $\sim 11,000$ ms including robot motion.

In our pipeline, this latency has limited impact on overall task completion for three reasons. First, active disambiguation is triggered only when $p_{\text{amb}} > \tau$. Second, disambiguation is performed only at grasp initialization or after pose-loss recovery, rather than inside the high-frequency tracking loop. Third, the compute time within an NBV cycle is dominated by M sequential VLM queries for candidate ranking, which increases the *time-to-disambiguate* but does not affect per-step tracking control once a reliable pose is obtained.

Overall, while VLM queries remain the main bottleneck for faster disambiguation, they are not on the critical path of per-step tracking control and thus do not materially hinder manipulation in our scenarios.

E. Engineering Case Study: Peg-in-Hole Assembly

Beyond isolated estimation and tracking, we evaluate a peg-in-hole assembly task as an *engineering case study* to demonstrate the practical utility of ActivePose in a closed-loop manipulation pipeline. In each run, the robot grasps the object from the tabletop and inserts it into a fixed socket whose position is randomized. We use the assembly policy from [36], which takes as input the relative SE(3) pose between the grasped object and the socket and outputs short-horizon end-effector motions to complete the assembly task. ActivePose provides this relative pose online by combining (i) active disambiguation at grasp initialization and (ii) active tracking during insertion to maintain visibility under motion and occlusions. This setting jointly tests reliable initialization (resolving grasp-time ambiguity) and sustained visibility during insertion.

Baselines and metric. We compare against three baselines: **Fixed-View + World-Camera** (single estimate from a fixed world camera), **Fixed-View + Pose-Servo** (single estimate at grasp followed by pose-based visual servoing during insertion), and **Random-NBV + Pose-Servo** (one random feasible NBV at grasp for a second estimate, then pose-servo during insertion). We report success rate (SR) as

the fraction of trials that complete the insertion (20 trials per method).

Results and discussion. Table V shows that ActivePose achieves the best performance (90%). Fixed-View + World-Camera often fails when the randomized socket falls outside the fixed FOV (40%), while Fixed-View + Pose-Servo is limited by reachability and pose-loss during insertion (50%). Random-NBV + Pose-Servo reduces grasp-time ambiguity and improves SR to 70%, but still suffers from pose-loss under a fixed-view servo controller. By actively disambiguating at grasp and tracking during insertion, ActivePose maintains visibility and provides reliable relative poses for the downstream insertion.

VI. CONCLUSION

In this work, we propose *ActivePose*, a closed-loop framework that combines zero-shot active pose estimation with active camera tracking for robotic manipulation. Our method performs pose estimation by grounding a VLM with entropy-ranked CAD renderings and selecting disambiguating NBVs, and then performs tracking to maintain visibility during manipulation using a diffusion-policy tracker to prevent pose-loss under motion and occlusions. Experiments in simulation and on real dual-arm hardware show consistent improvements over baselines, and an industrial peg-in-hole assembly case study demonstrates practical benefits in a closed-loop manipulation pipeline.

REFERENCES

- [1] C. Choi, W. Schwarting, J. DelPreto, and D. Rus, "Learning object grasping for soft robot hands," *IEEE Robotics and Automation Letters*, vol. 3, no. 3, pp. 2370–2377, 2018.
- [2] H.-S. Fang, C. Wang, M. Gou, and C. Lu, "Graspnet-1billion: A large-scale benchmark for general object grasping," in *Proceedings of the IEEE/CVF conference on computer vision and pattern recognition*, pp. 11444–11453, 2020.
- [3] X. Zhang, W. Lv, and L. Zeng, "A 6dof pose estimation dataset and network for multiple parametric shapes in stacked scenarios," *Machines*, vol. 9, no. 12, p. 321, 2021.
- [4] A. A. Malik, M. V. Andersen, and A. Bilberg, "Advances in machine vision for flexible feeding of assembly parts," *Procedia Manufacturing*, vol. 38, pp. 1228–1235, 2019.
- [5] S. Peng, Y. Liu, Q. Huang, X. Zhou, and H. Bao, "Pvnet: Pixel-wise voting network for 6dof pose estimation," in *Proceedings of the IEEE/CVF Conference on Computer Vision and Pattern Recognition*, pp. 4561–4570, 2019.
- [6] S. Zakharov, I. Shugurov, and S. Ilic, "Dpod: 6d pose object detector and refiner," in *Proceedings of the IEEE/CVF international conference on computer vision*, pp. 1941–1950, 2019.
- [7] Z. Li, G. Wang, and X. Ji, "Cdpn: Coordinates-based disentangled pose network for real-time rgb-based 6-dof object pose estimation," in *Proceedings of the IEEE/CVF International Conference on Computer Vision*, pp. 7678–7687, 2019.
- [8] J. Cheng, P. Liu, Q. Zhang, H. Ma, F. Wang, and J. Zhang, "Real-time and efficient 6-d pose estimation from a single rgb image," *IEEE Transactions on Instrumentation and Measurement*, vol. 70, pp. 1–14, 2021.
- [9] G. Wang, F. Manhardt, F. Tombari, and X. Ji, "Gdr-net: Geometry-guided direct regression network for monocular 6d object pose estimation," in *Proceedings of the IEEE/CVF Conference on Computer Vision and Pattern Recognition*, pp. 16611–16621, 2021.
- [10] G. Zhou, D. Wang, Y. Yan, C. Liu, and Q. Chen, "6-d object pose estimation using multiscale point cloud transformer," *IEEE Transactions on Instrumentation and Measurement*, vol. 72, pp. 1–11, 2022.
- [11] V. N. Nguyen, T. Groueix, M. Salzmann, and V. Lepetit, "Gigapose: Fast and robust novel object pose estimation via one correspondence," in *Proceedings of the IEEE/CVF Conference on Computer Vision and Pattern Recognition*, pp. 9903–9913, 2024.
- [12] B. Wen, W. Yang, J. Kautz, and S. Birchfield, "Foundationpose: Unified 6d pose estimation and tracking of novel objects," in *Proceedings of the IEEE/CVF Conference on Computer Vision and Pattern Recognition*, pp. 17868–17879, 2024.
- [13] J. Lin, L. Liu, D. Lu, and K. Jia, "Sam-6d: Segment anything model meets zero-shot 6d object pose estimation," in *Proceedings of the IEEE/CVF Conference on Computer Vision and Pattern Recognition*, pp. 27906–27916, 2024.
- [14] T. Höfer, B. Kiefer, M. Messmer, and A. Zell, "Hyperposepdf-hypernetworks predicting the probability distribution on so (3)," in *Proceedings of the IEEE/CVF Winter Conference on Applications of Computer Vision*, pp. 2369–2379, 2023.
- [15] K. Murphy, C. Esteves, V. Jampani, S. Ramalingam, and A. Makadia, "Implicit-pdf: Non-parametric representation of probability distributions on the rotation manifold," *arXiv preprint arXiv:2106.05965*, 2021.
- [16] J. Sock, G. Garcia-Hernando, and T.-K. Kim, "Active 6d multi-object pose estimation in cluttered scenarios with deep reinforcement learning," in *2020 IEEE/RSJ International Conference on Intelligent Robots and Systems (IROS)*, pp. 10564–10571, 2020.
- [17] J. Yang, W. Xue, S. Ghavidel, and S. L. Waslander, "Active 6d pose estimation for textureless objects using multi-view rgb frames," 2025.
- [18] T. Mizuno, K. Yabashi, and T. Tasaki, "Object pose estimation by camera arm control based on the next viewpoint estimation," in *2024 IEEE/RSJ International Conference on Intelligent Robots and Systems (IROS)*, p. 9482–9487, IEEE, Oct. 2024.
- [19] K. Park, T. Patten, and M. Vincze, "Pix2pose: Pixel-wise coordinate regression of objects for 6d pose estimation," in *Proceedings of the IEEE/CVF International Conference on Computer Vision*, pp. 7668–7677, 2019.
- [20] Y. He, W. Sun, H. Huang, J. Liu, H. Fan, and J. Sun, "Pvn3d: A deep point-wise 3d keypoints voting network for 6dof pose estimation," 2020.
- [21] I. Shugurov, S. Zakharov, and S. Ilic, "Dpodv2: Dense correspondence-based 6 dof pose estimation," *IEEE Transactions on Pattern Analysis and Machine Intelligence*, vol. 44, no. 11, pp. 7417–7435, 2022.
- [22] T. Hodaň, M. Sundermeyer, B. Drost, Y. Labbé, E. Brachmann, F. Michel, C. Rother, and J. Matas, "Bop challenge 2020 on 6d object localization," in *Computer Vision—ECCV 2020 Workshops: Glasgow, UK, August 23–28, 2020, Proceedings, Part II 16*, pp. 577–594, Springer, 2020.
- [23] R. Shao, W. Li, L. Zhang, R. Zhang, Z. Liu, R. Chen, and L. Nie, "Large vlm-based vision-language-action models for robotic manipulation: A survey," 2025.
- [24] D. Driess, F. Xia, M. S. M. Sajjadi, C. Lynch, A. Chowdhery, B. Ichter, A. Wahid, J. Tompson, Q. Vuong, T. Yu, W. Huang, Y. Chebotar, P. Sermanet, D. Duckworth, S. Levine, V. Vanhoucke, K. Hausman, M. Toussaint, K. Greff, A. Zeng, I. Mordatch, and P. Florence, "Palm-e: An embodied multimodal language model," 2023.
- [25] J. Liang, W. Huang, F. Xia, P. Xu, K. Hausman, B. Ichter, P. Florence, and A. Zeng, "Code as policies: Language model programs for embodied control," 2023.
- [26] S. Vemprala, R. Bonatti, A. Buckner, and A. Kapoor, "Chatgpt for robotics: Design principles and model abilities," 2023.
- [27] X. Li, M. Liu, H. Zhang, C. Yu, J. Xu, H. Wu, C. Cheang, Y. Jing, W. Zhang, H. Liu, H. Li, and T. Kong, "Vision-language foundation models as effective robot imitators," 2024.
- [28] S. Wang, S. Liu, W. Wang, J. Shan, and B. Fang, "Robobert: An end-to-end multimodal robotic manipulation model," 2025.
- [29] M. J. Kim, K. Pertsch, S. Karamcheti, T. Xiao, A. Balakrishna, S. Nair, R. Rafailov, E. Foster, G. Lam, P. Sanketi, Q. Vuong, T. Kollar, B. Burchfiel, R. Tedrake, D. Sadigh, S. Levine, P. Liang, and C. Finn, "Openvla: An open-source vision-language-action model," 2024.
- [30] R. Wolf, Y. Shi, S. Liu, and R. Rayyes, "Diffusion models for robotic manipulation: A survey," 2025.
- [31] C. Chi, Z. Xu, S. Feng, E. Cousineau, Y. Du, B. Burchfiel, R. Tedrake, and S. Song, "Diffusion policy: Visuomotor policy learning via action diffusion," 2024.
- [32] J. Song, C. Meng, and S. Ermon, "Denosing diffusion implicit models," 2022.

- [33] G. Wang, F. Manhardt, F. Tombari, and X. Ji, "Gdr-net: Geometry-guided direct regression network for monocular 6d object pose estimation," in *2021 IEEE/CVF Conference on Computer Vision and Pattern Recognition (CVPR)*, pp. 16606–16616, 2021.
- [34] J. Panerati, H. Zheng, S. Zhou, J. Xu, A. Prorok, and A. P. Schoellig, "Learning to fly – a gym environment with pybullet physics for reinforcement learning of multi-agent quadcopter control," 2021.
- [35] L. Chen, H. Yang, C. Wu, and S. Wu, "Mp6d: An rgb-d dataset for metal parts' 6d pose estimation," *IEEE Robotics and Automation Letters*, vol. 7, no. 3, pp. 5912–5919, 2022.
- [36] H. Sun, Y. Wang, Z. Zhou, S. Wang, H. Yang, J. Sun, and Q. Cao, "Exploring pose-guided imitation learning for robotic precise insertion," 2025.